



Undergraduate Honors Theses

2024-07-14

An Information Geometric Analysis of a Shallow-Water Waveguide Using VGS Parametrization

Michelle Wang

Follow this and additional works at: https://scholarsarchive.byu.edu/studentpub_uht

BYU ScholarsArchive Citation

Wang, Michelle, "An Information Geometric Analysis of a Shallow-Water Waveguide Using VGS Parametrization" (2024). *Undergraduate Honors Theses*. 401.
https://scholarsarchive.byu.edu/studentpub_uht/401

This Honors Thesis is brought to you for free and open access by BYU ScholarsArchive. It has been accepted for inclusion in Undergraduate Honors Theses by an authorized administrator of BYU ScholarsArchive. For more information, please contact ellen_amatangelo@byu.edu.

Honors Thesis

AN INFORMATION GEOMETRIC ANALYSIS OF A SHALLOW-WATER
WAVEGUIDE USING VGS PARAMETRIZATION

by
Michelle S. Wang

Submitted to Brigham Young University in partial fulfillment
of graduation requirements for University Honors

Department of Physics and Astronomy
Brigham Young University
August 2024

Advisor: Dr. Tracianne B. Neilsen

Faculty Reader: Dr. Mark N. Transtrum

Honors Coordinator: Dr. Davi Obata

ABSTRACT

AN INFORMATION GEOMETRIC ANALYSIS OF A SHALLOW-WATER WAVEGUIDE USING VGS PARAMETRIZATION

Michelle S. Wang

Department of Physics and Astronomy

Bachelor of Science

In geoacoustic inversion, selecting an appropriate seabed parametrization, especially with an unknown number of sediment layers, is a challenge that is compounded by potential bias when establishing bounds in the parameter search space. One approach to addressing these issues is rooted in the techniques of information geometry. Information geometry informs model selection and parametrization by quantifying which model parameters are informed by observational data. This paper provides an information geometric analysis of a shallow-water waveguide, where the acoustic properties of the lower half-space are derived from the viscous grain-shearing (VGS) model.

Specifically, we consider single-frequency transmission loss (TL) across a wide range of VGS parameters. By exploring the limits and boundaries of the geometric manifolds, particularly as parameters approach both low and high extremes, this approach allows for the determination of relative stiffness and sloppiness of model parameters and provides indications of parameter hierarchies and correlations. Results include slices of the model manifold and matrices of information distances on a five-dimensional model manifold, representing the absolute transmission loss at 16 receiver depths for different sediment types. Careful examination of these results provides insights into the relative impact

of VGS parameters and the delineation of limiting regions. In doing so, this paper has uncovered a quandary about one of the parameters: how should the visco-elastic time constant change between the two empirically determined values of 0.12 ms for coarse sediments and infinity for fine-grained sediments? This work demonstrates how information geometry can inform model selection and parametrization in geoacoustic inversion studies, leading to more efficient and interpretable models of the seabed. [Work supported by the Office of Naval Research. Grant N00014-21-S-B001]

ACKNOWLEDGMENTS

I would like to express my sincerest gratitude to Dr. Traci Neilsen for her invaluable mentorship throughout my research journey. Her guidance, patience, and kindness have been instrumental in shaping my understanding of underwater acoustics and propelling my research forward. I am particularly grateful for her willingness to dedicate time to answer my questions to ensure my understanding and to always provide detailed, insightful feedback on my research direction. She is truly inspiring, and I am beyond grateful to have come under her mentorship. Words cannot adequately express my appreciation for Dr. Nielsen's unwavering support in shaping me as a researcher.

I am also deeply grateful for Dr. Mark Transtrum, who not only provided invaluable feedback throughout this study but also sparked a profound shift in my perspective on science. His lectures and reading materials in the course "Theory of Predictive Modeling" were instrumental in prompting me to contemplate the nature of science in new ways and reconsider fundamental concepts. I am thankful for the impact he has had on my journey as a hopeful scientist.

I would also like to extend my appreciation to Jay Spendlove who kindly introduced me to Dr. Neilsen and has dedicated so much of his time and effort to support me. I would also like to acknowledge the entire underwater acoustics group for their wonderful spirit and camaraderie.

Finally, I want to acknowledge my mother who has always been a pillar of support for me, lending me a priceless source of strength and motivation throughout all my endeavors.

Contents

| | |
|---|------------|
| Title | i |
| Abstract | iii |
| Acknowledgments | vi |
| List of Tables and Figures | x |
| 1 Introduction | 1 |
| 1.1 Information Geometry | 1 |
| 1.2 Sound Propagation in the Ocean | 2 |
| 1.3 Prior Work | 3 |
| 2 Methodology | 5 |
| 3 Results | 6 |
| 3.1 Process Overview and Parameter Exploration | 6 |
| 3.2 Visualization and Analysis of Model Manifolds | 10 |
| 3.3 Information Distances | 13 |
| 4 Conclusion | 21 |
| 5 Next Steps | 23 |
| 6 Appendix | 25 |
| References | 28 |

List of Figures

| | | |
|----|---|----|
| 1 | Mobius Strip Equations (left) and Model Manifold (right). | 2 |
| 2 | A sound propagation model. | 4 |
| 3 | Example model manifold in data space mapped from parameter space. Used with permission from authors. [7] | 5 |
| 4 | Description of VGS parameters for a sediment’s physical properties which are used to obtain values for ORCA acousto-elastic parameters. | 7 |
| 5 | Acousto-elastic parameters as functions of VGS parameters. | 8 |
| 6 | Real-world VGS parameter values for different sediment types, adapted from Knobles et al. “Inference of source signatures of merchant ships in shallow ocean environments” JASA (2024). | 9 |
| 7 | Parameter bounds and variations for modeling. | 9 |
| 8 | Expanded bounds for modeling. | 10 |
| 9 | TL model manifolds: 2-D slices when Porosity (N) vs. Strain Hard- ening Index (n) are varied, with rough granules as the base sediment type, for layer thickness = 20 m and source-receiver range = 3 km. (a) Colored lines on the parameter space plot correspond to the bound- aries of the model manifold. (b) Frequency = 100 Hz. (c) Frequency = 1000 Hz. | 12 |
| 10 | TL model manifolds: 2-D slices when Porosity (N) vs. Grain Bulk Modulus (K_g) are varied, with coarse silt as the base sediment type, for layer thickness = 20 m and source-receiver range = 3 km. (a) Frequency = 100 Hz. (b) Frequency = 1000 Hz. | 14 |
| 11 | TL model manifolds: 2-D slices when Porosity (N) vs. Viscous Time Constant (τ) are varied, with coarse silt as the base sediment type, for layer thickness = 20 m and source-receiver range = 9 km. (a) Frequency = 100 Hz. (b) Frequency = 1000 Hz. | 15 |

| | | |
|----|--|----|
| 12 | TL model manifolds: 2-D slices when Porosity (N) vs. Grain Density (ρ_g) are varied, with coarse silt as the base sediment type, for layer thickness = 20 m and frequency = 100 Hz. (a) Source-receiver range = 3 km. (b) Source-receiver range = 9 km. | 16 |
| 13 | Information Seabed Distances Matrix. Layer thickness = 20m, frequency = 100Hz, source-receiver range = 3km. | 18 |
| 14 | Information Seabed Distances Matrix, holding τ at its minimum value (0.12 ms) for all sediments. | 19 |
| 15 | Information Seabed Distances Matrix, holding τ at its maximum value (1111 s) for all sediments. | 20 |
| 16 | Information Seabed Distances Matrix with τ increasing logarithmically. | 22 |

1 Introduction

1.1 Information Geometry

In the realm of complex modeling and data analysis, understanding how model parameters influence predictions is crucial. Information geometry offers a robust framework for this purpose by leveraging concepts from differential geometry and statistics, providing insights into the structure of models and the relationship between parameters and data. In particular, information geometry aids in model selection by quantifying the information content that observational data provide about model parameters. This quantification allows for the determination of which parameters are essential and should be retained in the model and which parameters add little to no modeling value and can be excluded. This approach is particularly useful in complex models where not all parameters contribute equally to the accuracy and reliability of predictions.

Within the information geometry framework, model parameters can be categorized as stiff or sloppy. Stiff parameters are those that are well-constrained by the data, meaning small changes in these parameters can lead to significant changes in model predictions. In contrast, sloppy parameters are poorly constrained, where variations in these parameters result in negligible changes in model outcomes. Sloppiness can arise either because the parameters do not significantly influence the model or because certain combinations of parameters produce similar effects, making it difficult to isolate individual parameter contributions. As such, sloppy parameters can lead to ambiguous and unreliable model interpretations. By identifying and removing sloppy parameters, reduced models are obtained without sacrificing accuracy while offering improved robustness and interpretability.

Information geometry provides many tools to visualize and quantify parameter influence. For example, the Fisher Information Matrix (FIM) helps in understanding the curvature of the parameter space, which in turn indicates how sensitive the model



Figure 1: Mobius Strip Equations (left) and Model Manifold (right).

is to changes in each parameter. Parameters associated with high curvature regions are stiff, while those in flat regions are sloppy. In addition to the FIM, information geometry introduces the concept of a model manifold, which is the main tool used in this investigation.

In our exploration of a complex model's behavior, the model manifold serves as a geometric representation embedded within the data space. Just as the FIM provides a quantitative understanding of parameter sensitivity, the model manifold provides a visual and geometric perspective of how different parameter configurations affect the model's behavior.

Consider a two-parameter model wherein two parameters, u and v , define the model's behavior. These two parameters comprise the parameter space. As u and v are varied across their entire domains, we calculate a series of (x, y, z) points in the data space using the equations in Figure 1. Each combination of u and v maps to a specific (x, y, z) data outcome, mapping out the resulting model manifold and illustrating how changes in parameters translate to variations in model predictions. This thesis focuses on examining the model manifolds for sound propagation in the ocean.

1.2 Sound Propagation in the Ocean

The ability to accurately model and predict the behavior of sound underwater is crucial for a wide range of applications. Ocean experiments contain many complexi-

ties, such as the inherent difficulty of creating experimental datasets due to the time and expense. Compared to conducting extensive experimental studies, existing sound propagation models offer efficient alternatives. Two examples include the numerical normal mode models, such as ORCA, and analytical normal mode models like the Pekeris waveguide [6, 4] for simplified ocean environments.

Transmission loss (TL) is a fundamental parameter in underwater acoustics. TL refers to the decrease in acoustic energy as sound waves propagate through a medium. TL accounts for energy losses due to absorption, scattering, and spreading as sound waves travel. By quantifying how much acoustic energy is lost during propagation, TL provides insights into the impact of environmental factors on acoustic signal propagation. Factors include depth, temperature, and salinity of the water and sediment properties. These sediment properties intricately affect the reflectivity and absorptivity of the seafloor [3]. Understanding the impact of sediment properties on sound propagation is essential for deriving meaningful insights from acoustic data.

While the sediment properties are often represented as sound speed, density, and compressional attenuation, this work studies a more fundamental model: a sediment acoustics model known as Buckingham’s Viscous Grain Shearing (VGS) model. The VGS model serves as a valuable tool, providing physical bounds to the parameter space and offering insights into the frequency dependence of sound speed, attenuation, and naturally occurring marine sediments, such as mixtures of clay, silt, and sand. At present, the VGS model is likely the most general (causal) sediment acoustics model, capable of reasonably treating the broadest range of sediment fabrics [5].

1.3 Prior Work

In ocean acoustics, models are often sound propagation models like the ORCA model, which is an acoustic propagation model for multi-layered acousto-elastic ocean environments based on normal mode theory [9, 8]. As seen in Figure 2, the model assumes

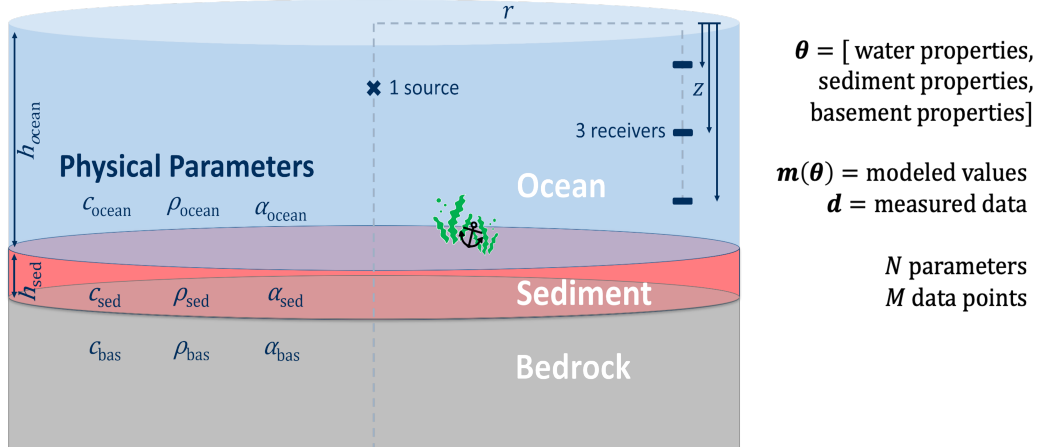


Figure 2: A sound propagation model.

the ocean is composed of a bedrock layer, a sediment layer, and an ocean layer, each with parameter values specific to it. For example, the sediment layer has parameters c_{sed} , ρ_{sed} , and α_{sed} , which respectively represent sound speed, density, and attenuation in the sediment. In this thesis, these parameters comprise the parameter space and the parameter vector θ . Each parameter combination used in the model yields a distinct modeled value at each receiver depth illustrated in Figure 2. Hence, the data space contains as many dimensions as the number of modeled values, which in this case is the number of receiver depths.

An example of previous work is shown in Figure 3. This model has a two-dimensional parameter space (Figure 3(a)), composed of density and sound speed. As the two parameters are varied across their domains, using a model like ORCA, when TL is calculated for two receiver depths, the model manifold is embedded in two-dimensional data space as shown in Figure 3(b). Evidently, this model is a non-linear transformation, as the square in parameter space becomes a ribbon in data space, and the relative distances between the sediment types marked by red crosses on the parameter space are changed on the model manifold.

The boundaries of the parameter space (Figure 3(a)) are color-coded here, allowing for a clear visualization of how the boundaries of the model manifold (similar colors

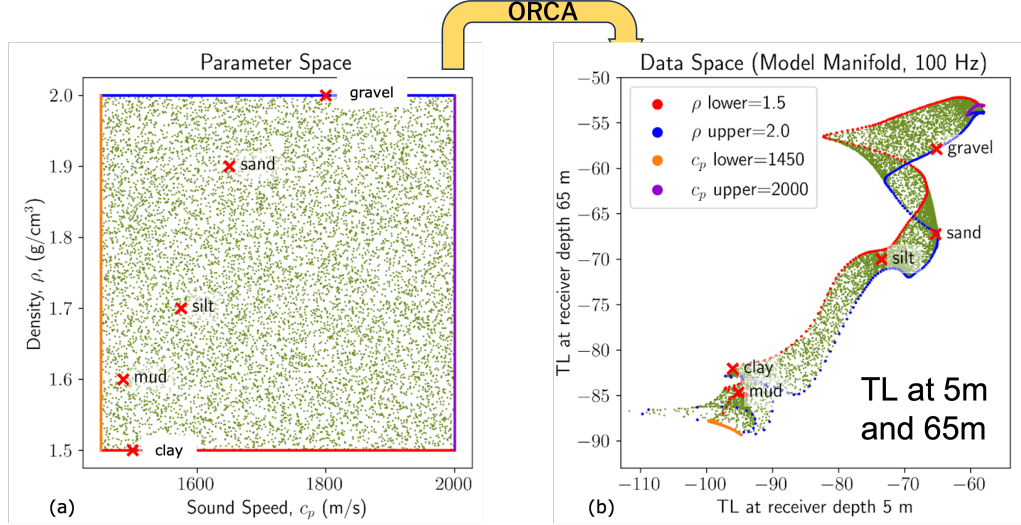


Figure 3: Example model manifold in data space mapped from parameter space. Used with permission from authors. [7]

in Figure 3(b)) correspond to a reduced-order model. From the parameter space box, observe that the orange line represents the variation in density as sound speed is held at its lowest value, and the purple line represents the variation in density as sound speed is held at its highest value. The red line represents the variation in sound speed as density is held at its lowest value, and the blue line represents the variation in sound speed as density is held at its highest value. On the model manifold, as both the orange and purple lines are significantly smaller than the red and blue, we observe then that the variation in density has less of an impact on the model manifold. In other words, density is a fairly sloppy parameter. In general, the thinner parts of the manifold correspond to where the model is sloppy.

2 Methodology

This work considers TL calculated from the ORCA normal mode model using the depth-dependent VGS parametrization of the sediment instead of directly from acousto-elastic parameters like sound speed and density. The table in Figure 4 describes each

VGS parameter. Some are related to the grains and some to the fluid between the grains. Others are constant reference parameters.

We consider the variations of the five VGS parameters $[N, \rho_g, K_g, n, \tau]$, in particular, which respectively describe a sediment layer’s properties of porosity, grain density, grain bulk modulus, strain hardening index, and the VGS time constant. All other parameters are held constant. These VGS parameters are fed into the equations in Figure 5 to yield the acousto-elastic parameters $[\rho, c_p, \alpha_p, c_s, \alpha_s]$, which are, respectively, sediment bulk density, compressional (sound) speed, compressional wave attenuation coefficient, shear wave sound speed, and shear wave attenuation coefficient. These acousto-elastic parameters are then input into the ORCA model to calculate TL at specified receiver depths, source-receiver ranges, and frequencies.

The goal is to explore the full parameter space by varying all five VGS parameters, effectively examining a five-dimensional manifold. However, visualizing this high-dimensional space directly is not feasible. Instead, two-dimensional slices of the model manifold are obtained by varying two parameters at a time while keeping the other three parameters fixed. These slices of the model manifold are created and examined for the sediment types of rough granules, coarse silt, and very soft clay.

For context, a table of possible real-world values for the VGS parameters at 16 different types of sediments is presented in Figure 6. This approach allows us to analyze the influence of individual parameters and their interactions within a manageable framework.

3 Results

3.1 Process Overview and Parameter Exploration

The bounds of the five VGS parameters that were varied to obtain model manifold slices are shown in Figure 7, along with other fixed values and specific cases examined.

| Parameter | Name | SI Units |
|----------------|---------------------------------|-------------------|
| N | Porosity | — |
| N_0 | Reference Porosity | — |
| ρ_w | Bottom Water Density | kg/m ³ |
| K_w | Bottom Water Bulk Modulus | Pa |
| ρ_g | Grain Density | kg/m ³ |
| K_g | Grain Bulk Modulus | Pa |
| μ_0 | Reference Grain Diameter | μm |
| $\gamma_{p,0}$ | Reference Compressional Modulus | Pa |
| $\gamma_{s,0}$ | Reference Shear Modulus | Pa |
| n | Strain Hardening Index | — |
| τ | VGS Time Constant | s |
| τ_0 | Reference Time Constant | s |
| Δ | Roughness Parameter | μm |
| T | Sediment Thickness | m |
| z | Depth | m |
| z_0 | Reference Depth | m |

Figure 4: Description of VGS parameters for a sediment's physical properties which are used to obtain values for ORCA acousto-elastic parameters.

$$\begin{aligned}
\rho &= N\rho_w + (1-N)\rho_g. \\
c_p &= c_0 \left(\Re \left\{ (1 + \chi g(\omega)(i\omega)^n)^{-1/2} \right\} \right)^{-1}, \\
\alpha_p &= -20 \log_{10}(e) \left(\frac{\omega}{c_0} \right) \Im \left\{ (1 + \chi g(\omega)(i\omega)^n)^{-1/2} \right\}, \\
c_s &= \frac{(\omega \tau_0)^{n/2}}{\cos(n\pi/4)} \sqrt{\frac{\gamma_s}{\rho}}, \\
\alpha_s &= 20 \log_{10}(e) \frac{(\omega \tau_0)^{1-n/2} \sin(n\pi/4)}{\tau_0} \sqrt{\frac{\rho}{\gamma_s}}. \\
\gamma_p &= \gamma_{p0} \left[\frac{(1-N)duH^{-1}}{(1-N_0)d_0u_0H_0^{-1}} \right]^{1/3}, \quad \chi = \frac{\gamma_p + (4/3)\gamma_s}{\rho c_0^2} \\
\gamma_s &= \gamma_{s0} \left[\frac{(1-N)duH^{-1}}{(1-N_0)d_0u_0H_0^{-1}} \right]^{2/3}, \quad g(\omega) = \left(1 + \frac{1}{i\omega\tau} \right)^{n-1}, \\
H &= E/(1 - \sigma^2), \quad \omega = 2\pi f : \text{angular frequency} = \text{constant}
\end{aligned}$$

Figure 5: Acousto-elastic parameters as functions of VGS parameters.

In this study, two VGS parameters are varied across their entire domains while keeping the other three fixed at values from Figure 6 appropriate for the base sediment type under consideration. This was performed for all possible two-parameter combinations. Additionally, the following parameters were held constant throughout the investigation: water depth h_w , source depth z_s , water sound speed c_w , and receiver depth z_r .

Each two-parameter variation was examined across eight different cases, where frequency was adjusted to be either 100 Hz or 1000 Hz, source-receiver range to be 3 km or 9 km, and layer thickness to be either 20 m or 200 m. For example, one case under which all possible two-parameter variations were examined was frequency = 100 Hz, source-receiver range = 3 km, and layer thickness = 20 m. Another case was frequency = 100 Hz, source-receiver range = 3 km, and layer thickness = 200 m.

This process was repeated for three base sediment types from Figure 6, resulting

| Sediment Type | N | ρ_g | K_g | n | τ |
|----------------------|----------|----------|-------|----------|---------|
| rough granules | 0.372 | 2650 | 36 | 0.12 | 0.00012 |
| granules | 0.372 | 2650 | 36 | 0.12 | 0.00012 |
| very coarse sand | 0.374 | 2650 | 36 | 0.111 | 0.00012 |
| coarse sand | 0.378 | 2650 | 32 | 0.1 | 0.00012 |
| medium sand | 0.385 | 2650 | 28 | 0.095 | 0.00012 |
| fine sand | 0.399 | 2600 | 28 | 0.085 | 0.00012 |
| very fine sand | 0.425 | 2600 | 28 | 0.08 | 0.00012 |
| coarse silt | 0.471 | 2550 | 22 | 0.07 | 0.00012 |
| silty sand | 0.5 | 2600 | 19 | 0.0775 | 0.0012 |
| medium silt | 0.543 | 2525 | 14.67 | 0.067 | 0.012 |
| clayey sandy silt | 0.6 | 2500 | 13.67 | 0.065 | 1111 |
| fine silt | 0.64 | 2500 | 13.61 | 0.06 | 1111 |
| silty clay | 0.694 | 2500 | 13.55 | 0.0575 | 1111 |
| very fine silt | 0.735 | 2500 | 13.5 | 0.055 | 1111 |
| clay | 0.75 | 2500 | 13.5 | 0.05 | 1111 |
| very soft clay | 0.9 | 2400 | 8.85 | 0.045 | 1111 |

Figure 6: Real-world VGS parameter values for different sediment types, adapted from Knobles et al. “Inference of source signatures of merchant ships in shallow ocean environments” JASA (2024).

| Parameter | Bounds | Fixed Values | Cases: |
|------------------|-----------------|---------------------|-------------------------|
| N | [0.372, 0.9] | h_w = 100m | freqs: 100Hz, 1000Hz |
| ρ_g | [2400, 2650] | z_s = 10m | src-rec range: 3km, 9km |
| K_g | [8.85, 36] | c_w = 1500m/s | h_1: 20m, 200m |
| n | [0.045, 0.12] | z_r = 20, 50, 80m | |
| τ | [0.00012, 1111] | | |

Figure 7: Parameter bounds and variations for modeling.

| Parameter | Expanded Bounds | Fixed Values | Cases: |
|-----------|-----------------|----------------------------|-------------------------|
| N | [0.372, 0.999] | $h_w = 100\text{m}$ | freqs: 100Hz, 1000Hz |
| ρ_g | [1050, 4000] | $z_s = 10\text{m}$ | src-rec range: 3km, 9km |
| K_g | [1, 60] | $c_w = 1500\text{m/s}$ | h_1 : 20m, 200m |
| n | [0.001, 1.0] | $z_r = 20, 50, 80\text{m}$ | |
| τ | [0.00001, 1e5] | | |

Figure 8: Expanded bounds for modeling.

in a comprehensive analysis across the three different sediment types rough granules, coarse silt, and very soft clay. The goal was to capture the behavior of the model manifold under various conditions and parameter settings, ensuring a robust understanding of the transmission loss characteristics across different scenarios.

To explore the model’s behavior beyond typical physical regimes and to understand the sensitivity and robustness of the VGS model under more extreme conditions, the analysis was repeated using expanded bounds, as shown in Figure 8. By extending the parameter ranges beyond their usual physical limits, we aimed to investigate potential nonlinear effects and any emergent phenomena that could provide deeper insights into the model’s behavior and performance.

Thus, for each of the three base sediment types, this study evaluated the eight cases utilizing physical bounds and eight cases employing expanded bounds. Ten two-parameter variation combinations are explored within each case, with each combination yielding a two-dimensional slice of the five-dimensional model manifold.

3.2 Visualization and Analysis of Model Manifolds

A comprehensive set of 480 model manifolds was generated, each depicting different parameter combinations and their effects on TL. Selected examples that highlight general trends and significant insights into parameter sensitivity will be discussed.

One such example is the model manifold in Figure 9 obtained from varying poros-

ity (N) and the strain hardening index (n). The color-coded parameter space box depicted in Figure 9(a) is the reference for interpreting subsequent discussions. In this convention, the first parameter named in the caption is designated as θ_1 and the second parameter is designated as θ_2 . This notation is consistently applied throughout the following analysis.

The model manifolds in Figures 9(b) and 9(c) offer valuable insights into the relative impacts of porosity (N) and strain hardening index (n) on TL. The extensive spread exhibited by the purple and yellow lines underscores the significant dependence of TL on porosity variations. In contrast, the red and blue lines, representing different strain hardening index values at fixed porosity levels, are noticeably shorter, suggesting that, compared to porosity, strain hardening index has a relatively weaker influence on TL.

Interestingly, the red and blue lines for the 1000 Hz case display a wider spread of TL values compared to the 100 Hz case. This observation suggests that strain hardening index might exhibit a more nuanced influence on TL at higher frequencies, even though its overall effect remains smaller compared to porosity. However, the fact that these lines remain relatively short across different manifolds indicates that strain hardening index is a fairly sloppy parameter.

As a second example, Figure 10 shows two model manifolds obtained from varying porosity (N) and grain bulk modulus (K_g). Similar to the observations in Figure 9, the extensive spread of the yellow and purple lines highlights the significant dependence of TL on porosity variations. The relatively short red line indicates that grain bulk modulus has a weaker overall impact on TL compared to porosity. However, unlike the previous example where the blue line exhibited minimal variation, the blue line in Figure 10 displays a noticeable spread in TL values. This suggests that grain bulk modulus can have a significant influence on TL and is a much stiffer parameter at low porosity than high porosity.

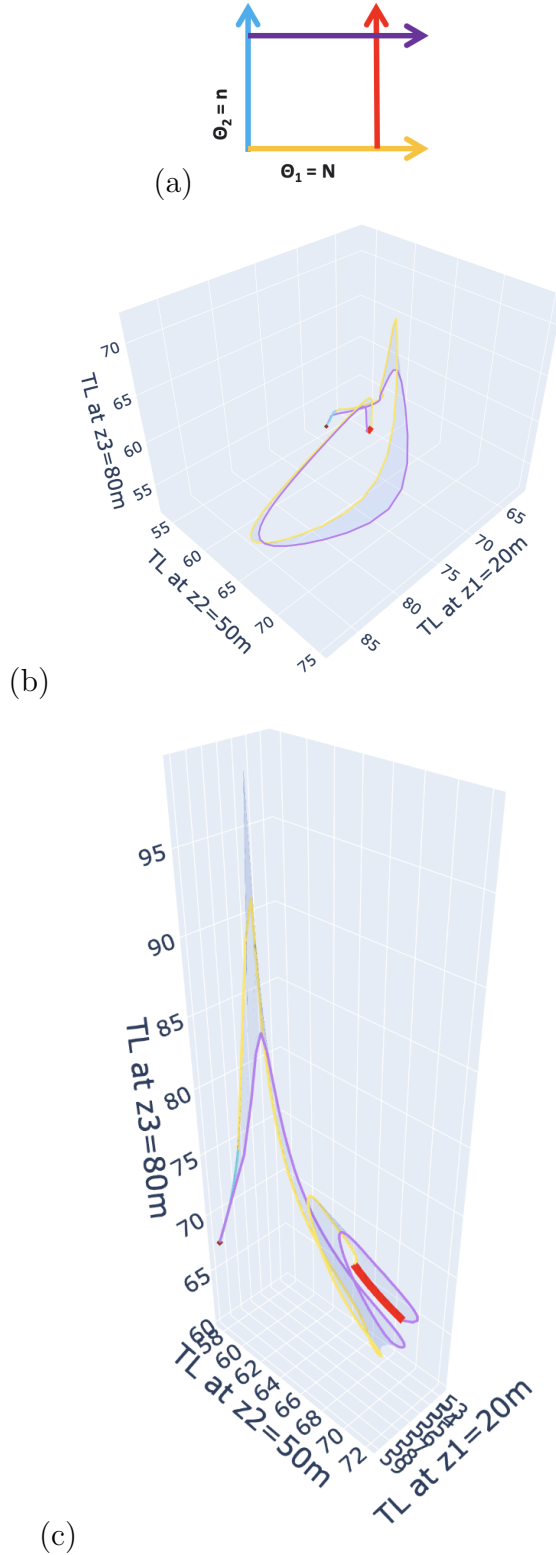


Figure 9: TL model manifolds: 2-D slices when Porosity (N) vs. Strain Hardening Index (n) are varied, with rough granules as the base sediment type, for layer thickness = 20 m and source-receiver range = 3 km. (a) Colored lines on the parameter space plot correspond to the boundaries of the model manifold. (b) Frequency = 100 Hz. (c) Frequency = 1000 Hz.

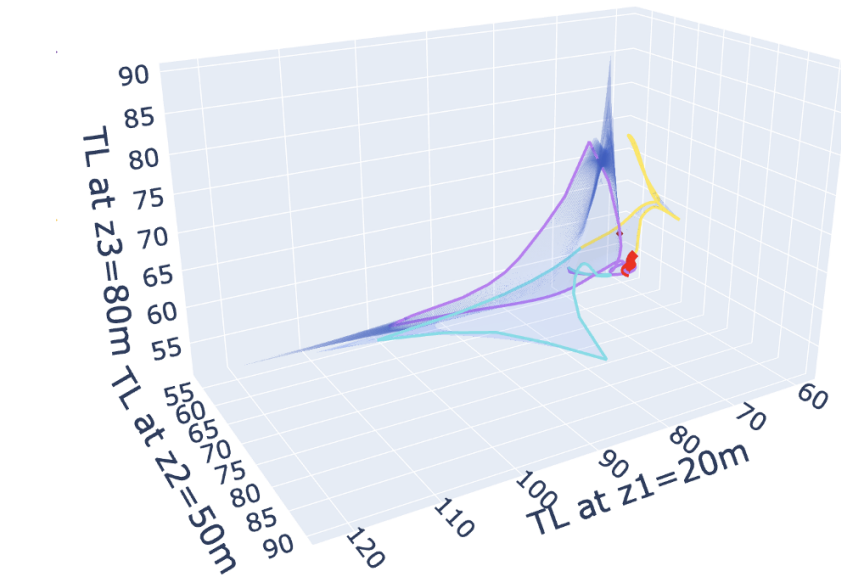
Furthermore, another general trend has been identified across multiple manifolds: the model manifolds for the 1000 Hz case consistently appear to be narrower compared to their 100 Hz counterparts. This difference suggests that the influence of various parameters on TL becomes more focused or condensed at higher frequencies.

The observation regarding the blue line’s extent at low porosity extends to other parameters as well. Figure 11 depicts a model manifold where porosity (N) and the viscous time constant (τ) are varied. The spread of the blue line, particularly at 100 Hz, highlights that, similar to grain bulk modulus, the viscous time constant can significantly impact TL at low porosity levels. So, the viscous time constant is a stiffer parameter at low porosity than at high porosity. In Figure 11, the yellow line, which represents the variation of porosity at the lowest viscous time constant, becomes not only shorter but spans a smaller range as the frequency increases. This underscores the earlier observation that model manifolds tend to become narrower as the frequency increases.

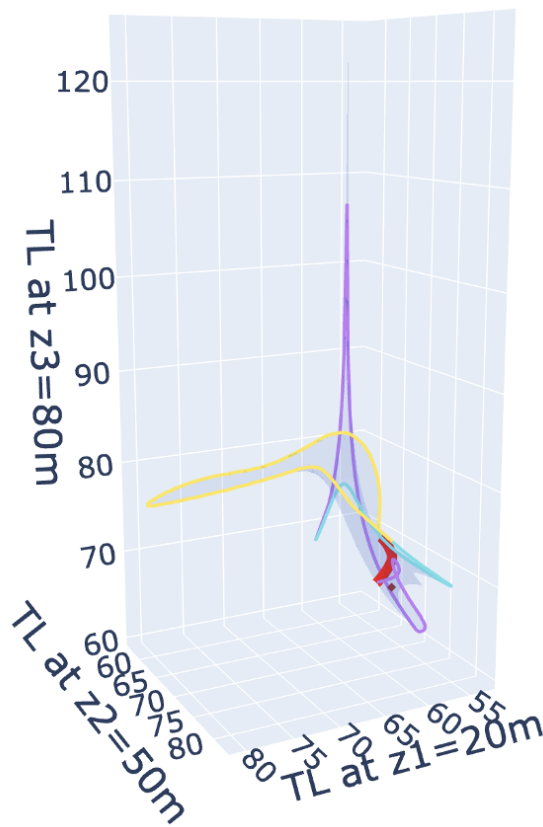
The impact of source-receiver range can be seen in Figure 12 where both manifolds are at 100 Hz but different ranges. As range increases, model manifolds exhibit increasing complexity, a trend observed consistently across all parameter variations. Additionally, as with the previous manifolds, porosity is stiffer than the grain density.

3.3 Information Distances

In addition to looking at the model manifolds to find sloppy parameters and other trends, the Euclidean distances between points on the five-dimensional model manifold can be calculated. The resulting information distances relate to the acoustic distinguishability between the modeled values corresponding to different modeling parameters. The acoustic distinguishability in TL at 16 receiver depths evenly spaced from 15.75 m to 72.0 m was calculated for 15 sediment types using the values in Figure 6. The roughness parameter of the sediment is not included, as both the rough



(a)



(b)

Figure 10: TL model manifolds: 2-D slices when Porosity (N) vs. Grain Bulk Modulus (K_g) are varied, with coarse silt as the base sediment type, for layer thickness = 20 m and source-receiver range = 3 km. (a) Frequency = 100 Hz. (b) Frequency = 1000 Hz.

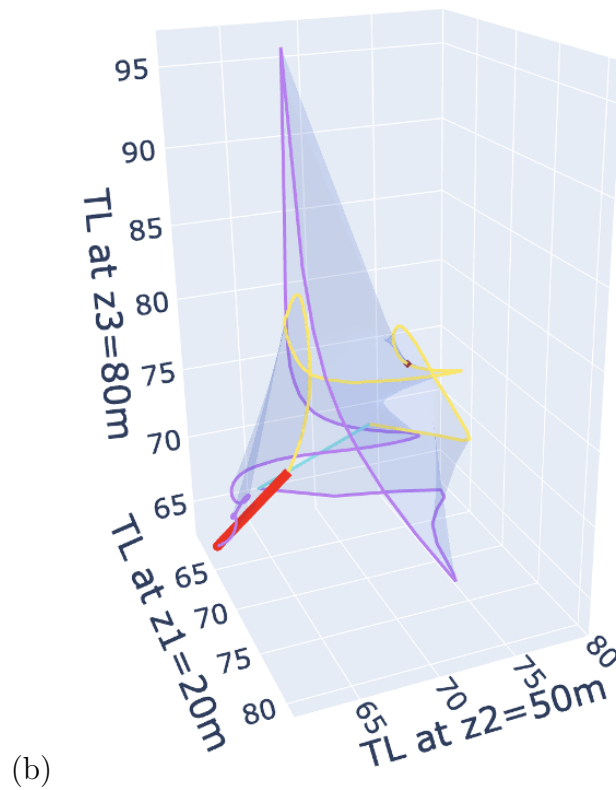
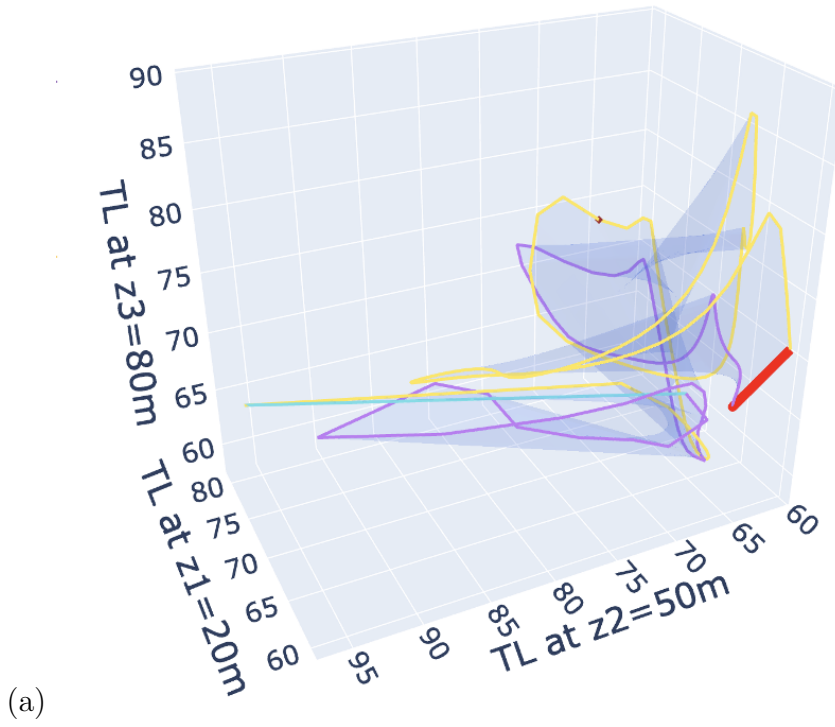
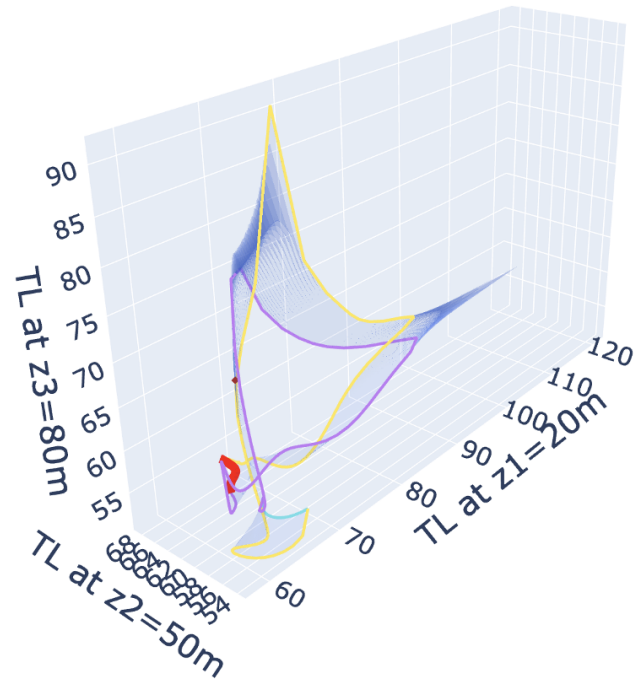
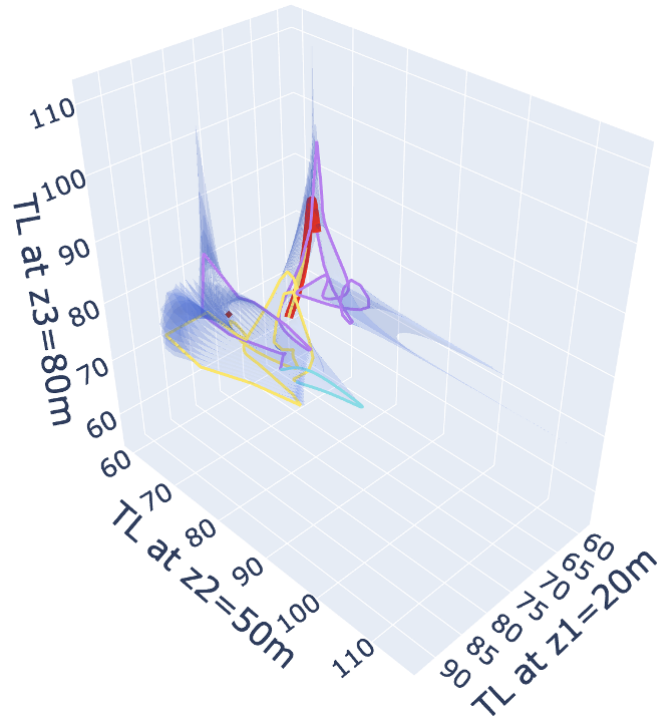


Figure 11: TL model manifolds: 2-D slices when Porosity (N) vs. Viscous Time Constant (τ) are varied, with coarse silt as the base sediment type, for layer thickness = 20 m and source-receiver range = 9 km. (a) Frequency = 100 Hz. (b) Frequency = 1000 Hz.



(a)



(b)

Figure 12: TL model manifolds: 2-D slices when Porosity (N) vs. Grain Density (ρ_g) are varied, with coarse silt as the base sediment type, for layer thickness = 20 m and frequency = 100 Hz. (a) Source-receiver range = 3 km. (b) Source-receiver range = 9 km.

granules sediment and the granules sediment share identical values. Using these transmission losses, across the different cases where frequency, range, and thickness were varied, an information distances matrix was created, which shows the relative distances between each sediment type. An example of such a matrix is shown in Figure 13.

This matrix provides a visual representation of how similar or different the transmission losses are between pairs of sediment types. The values in the matrix represent the relative distances, with smaller values indicating closer similarity and larger values indicating greater differences.

Upon examining the information distances matrix in Figure 13, unexpected discontinuities can be observed. Notably, for instance, silty sand appears to be closer to rough granules than to coarse silt or medium sand. These discontinuities are not what we would expect based on the physical properties of the sediments.

To investigate the cause of these anomalies, parameter values across the sediments of interest were examined. The evaluation found that changes in τ were responsible for these unphysical information distance situations. According to Knobles' table of VGS parameter values, τ does not transition progressively from one sediment type to another. Instead, it jumps from very small values of 0.12 ms to a value of 1111 s, which is chosen as a representation of infinity. This sudden change in τ significantly impacts the transmission loss, causing the observed discontinuities in the information distances matrix.

By isolating the impact of τ , it was confirmed that the observed anomalies in the information distances matrix were due to the non-progressive changes in τ . This observation was confirmed by recalculating the distance matrices with constant $\tau=0.12$ ms in Figure 14 and $\tau=1111$ s in Figure 15. These two limits were empirically found by Buckingham's 2007 [1] and 2020 [2] papers to match sandy and fine-grained sediments respectively. However, the transition of τ from one domain to another remains

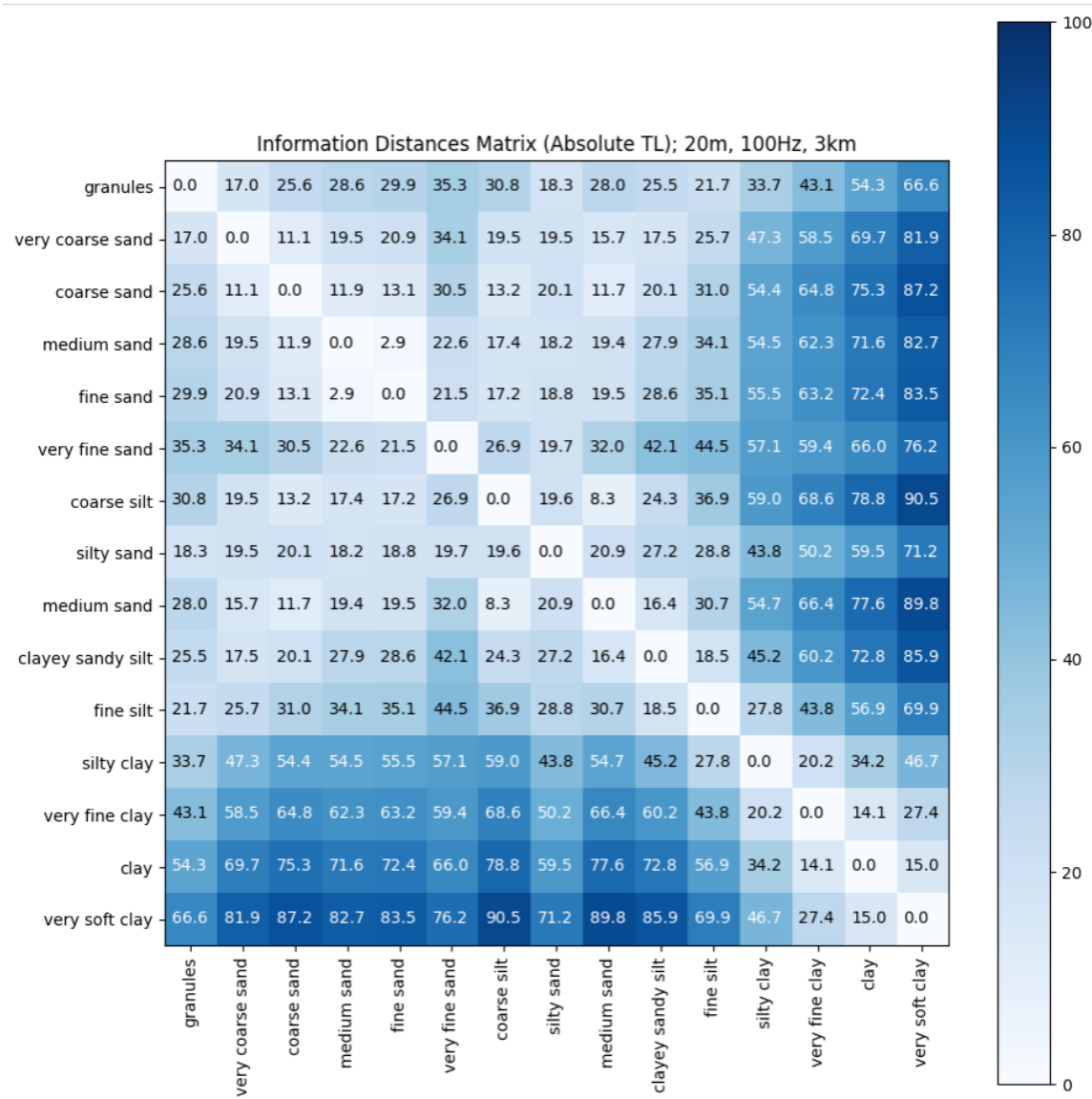


Figure 13: Information Seabed Distances Matrix.
 Layer thickness = 20m, frequency = 100Hz, source-receiver range = 3km.

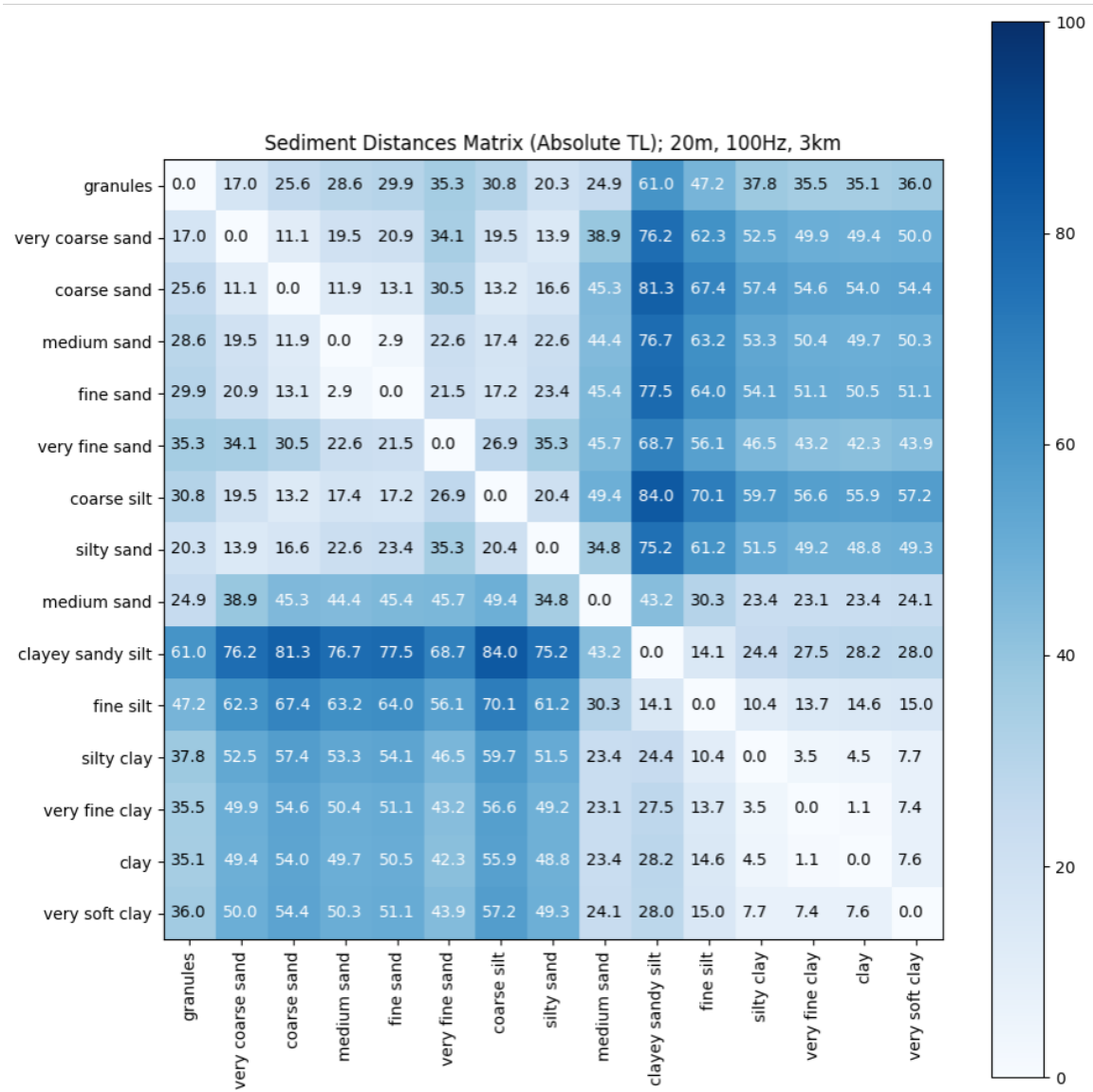


Figure 14: Information Seabed Distances Matrix, holding τ at its minimum value (0.12 ms) for all sediments.

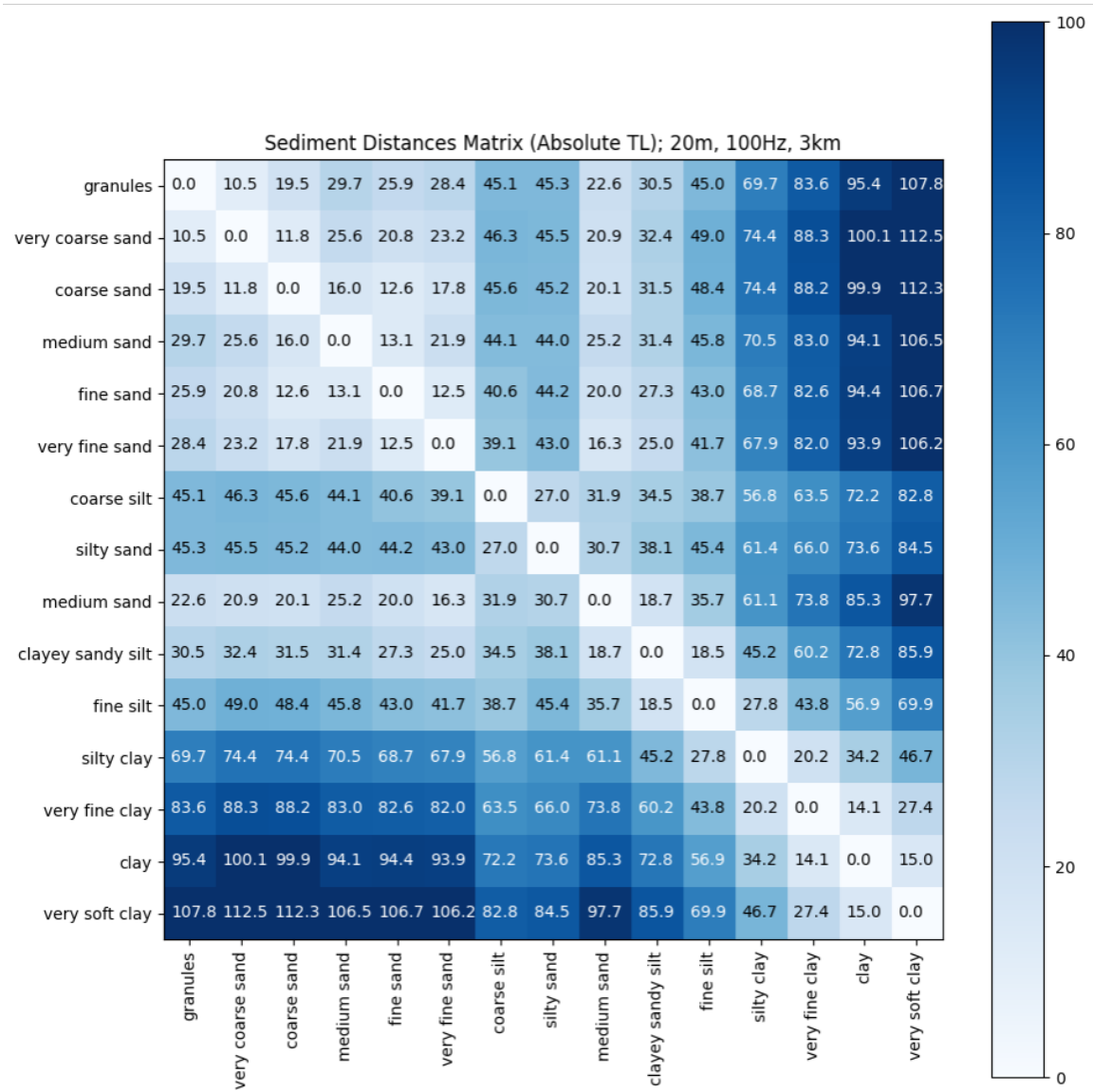


Figure 15: Information Seabed Distances Matrix, holding τ at its maximum value (1111 s) for all sediments.

an open research question. The band in the middle, where τ shifts between these two extremes, is not well understood. Is the change in τ truly discontinuous, or is there a continuous but complex process that governs this transition? One idea is to have τ change logarithmically, giving the information distances in Figure 16, which might provide a more realistic representation of the sediment transition. Exploring this approach could yield a more accurate and smooth matrix of information distances.

The discontinuities in Figure 13 suggest that the values provided in Knobles' table for τ may not be a realistic representation of the physical properties of the sediment types. Therefore, it is crucial to consider these findings when interpreting the transmission loss and information distances for various sediment types. This analysis also highlights the importance of carefully selecting and validating parameter values in sediment acoustics models to ensure accurate and realistic representations of acoustic propagation.

4 Conclusion

This study demonstrates the utility of information geometry as an approach for evaluating the sloppiness and stiffness of model parameters in the context of underwater acoustics. Through the application of information geometry, valuable insights have been gained into the structure of model manifolds and the relationship between parameters and data.

Specifically, the analysis of the Viscous Grain Shearing (VGS) model has revealed interesting findings regarding the complexity of the model manifold. It was observed that the complexity increases with range, highlighting the importance of considering spatial variations in acoustic propagation. Furthermore, porosity was identified as a relatively stiff parameter, suggesting its significant influence on model predictions. Conversely, parameters such as n exhibit a degree of sloppiness across the cases

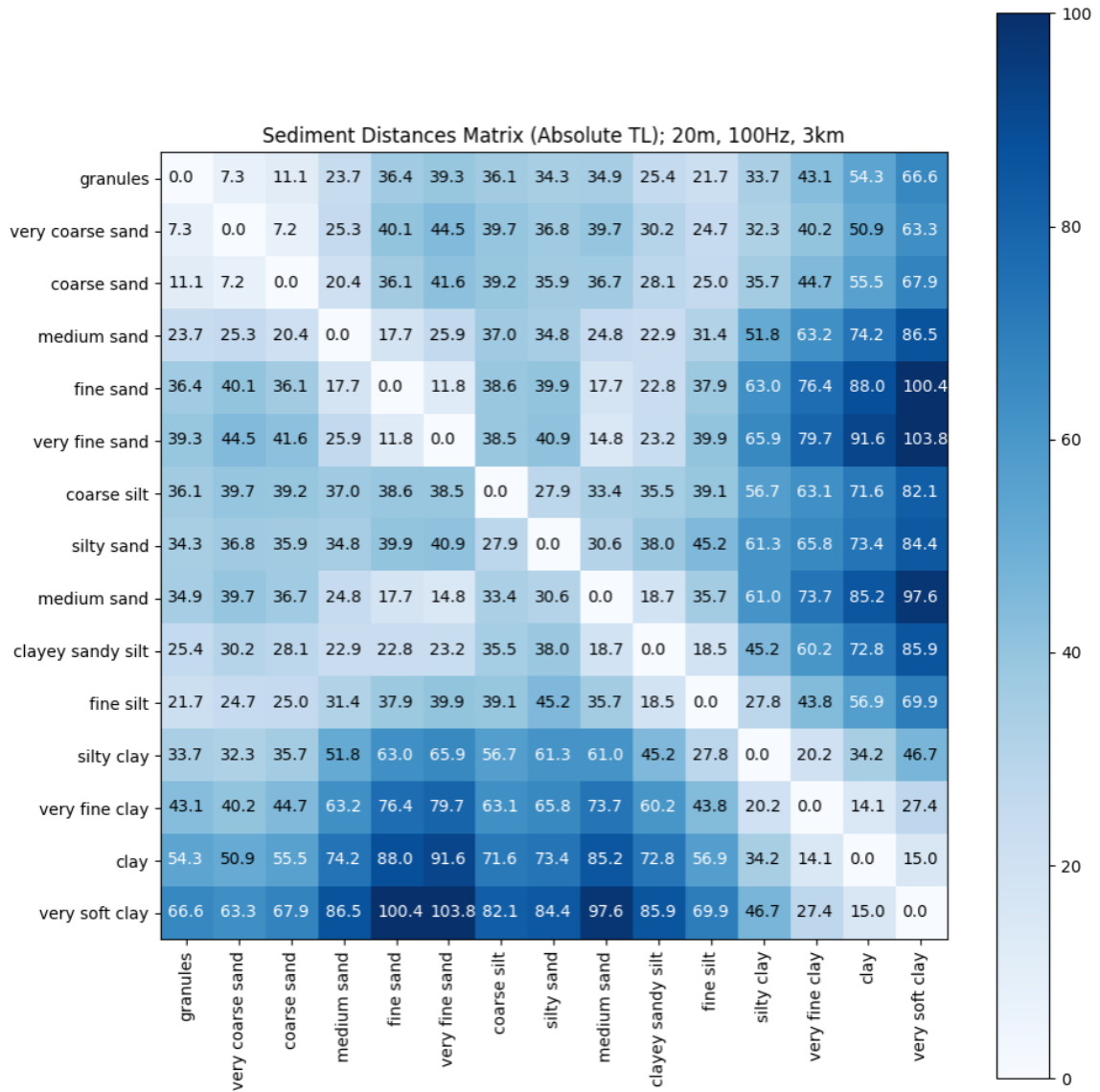


Figure 16: Information Seabed Distances Matrix with τ increasing logarithmically.

examined, indicating their limited impact on model outcomes.

These findings underscore the importance of considering parameter hierarchies and understanding the information content associated with different seabed parametrizations, particularly in the context of varying frequency and range. By leveraging information geometry, parameter influence can be effectively quantified, enabling informed decisions regarding model complexity and parameter selection.

This work also showed how information geometry can be used to check the acoustic similarities between modeling parameters using the information distance. In the cases studied here, the information revealed a difficulty in merging two empirical values for the limits of τ , which needs more investigation.

5 Next Steps

More research on optimal values for τ should be conducted to develop a methodology to transition smoothly between sediment types without disrupting the information distances. The goal is to integrate these refinements into the VGS model and ensure consistent, realistic representations of underwater acoustic propagation.

Further investigations across various sediment types are necessary to validate the observed trends and ensure their applicability across diverse environments. By systematically varying parameters across different sediment compositions, we aim to confirm the consistency of observed patterns and identify underlying principles that transcend specific sediment characteristics.

While this study focused on varying two parameters at a time, the next phase involves exploring the entire parameter space by simultaneously varying all five parameters. This transition to a truly five-dimensional manifold will utilize Principal Component Analysis (PCA) for visualization, allowing for a deeper understanding of parameter interactions and their influence on acoustic wave propagation.

An in-depth evaluation of boundary structures is also essential. By identifying regimes where a reduced-order model is appropriate, we can streamline model complexity without compromising accuracy. Additionally, we can leverage dimensionality reduction techniques, such as multidimensional scaling, to create a low-dimensional (e.g., 2D or 3D) embedding of the points in Euclidean space. This visual representation can provide valuable insights into the underlying structure of the data and potentially reveal hidden relationships that might be difficult to discern in the higher-dimensional space.

Finally, given the utilization of a half-space model for acoustic propagation, another next step involves shifting our focus from modeling transmission loss to investigating the reflection coefficient. This adjustment is motivated by the desire to gain deeper insights into how sound waves interact with boundaries, particularly at the sediment-water interface. The reflection coefficient quantifies the ratio of reflected acoustic energy to incident energy at a boundary interface, offering valuable insights into sound wave behavior, including phenomena like acoustic impedance mismatches and wave reflection.

6 Appendix

This appendix contains details about how to reproduce the results in this thesis.

Within `/home/byu.local/msw1998/underwater/michelle-wang/results` lives these four folders:

- `base_svp_coarse-silt`
- `base_svp_rough-granules`
- `base_svp_very-soft-clay`
- `sed_dist_matrix.abs.tl`

With the exception of the last folder listed above, which stores the information distances matrices for each case, each folder contains the following folders, which contain the model manifold plots for each parameter combination, saved as both a .PNG and a .HTML file. Additionally, for each parameter combination θ_1 and θ_2 , there are scatter plots of TL, calculated at each of the three receiver depths, as θ_1 is varied across its domain and θ_2 is held at either its highest or lowest value:

- `h1-20m_100Hz_3km_zs-10m`
- `h1-20m_100Hz_3km_zs-10m_expanded`
- `h1-20m_100Hz_9km_zs-10m`
- `h1-20m_100Hz_9km_zs-10m_expanded`
- `h1-20m_1000Hz_3km_zs-10m`
- `h1-20m_1000Hz_3km_zs-10m_expanded`
- `h1-20m_1000Hz_9km_zs-10m`

- h1-20m_1000Hz_9km_zs-10m_expanded
- h1-200m_100Hz_3km_zs-10m
- h1-200m_100Hz_3km_zs-10m_expanded
- h1-200m_100Hz_9km_zs-10m
- h1-200m_100Hz_9km_zs-10m_expanded
- h1-200m_1000Hz_3km_zs-10m
- h1-200m_1000Hz_3km_zs-10m_expanded
- h1-200m_1000Hz_9km_zs-10m
- h1-200m_1000Hz_9km_zs-10m_expanded

/home/byu.local/msw1998/underwater/michelle-wang/code/uw-library contains:

- .PKL files for each transmission loss grid calculated.
- Wang_InformationDistances.ipynb
 - Code to calculate and generate information distances matrices.
- Wang_VGS_TL_expanded-bounds-1.ipynb
 - Code to calculate and generate scatter plots and model manifolds using expanded bounds (part 1).
- Wang_VGS_TL_expanded-bounds-2.ipynb
 - Code to calculate and generate scatter plots and model manifolds using expanded bounds (part 2).

- `Wang_VGS_TL_original-bounds.ipynb`

- Code to calculate and generate scatter plots and model manifolds using original bounds.

All notebooks have been uploaded to the uw-library GitHub repository on the branch `michelle_honors_thesis`.

References

- [1] Michael J Buckingham. On pore-fluid viscosity and the wave properties of saturated granular materials including marine sediments. *The Journal of the Acoustical Society of America*, 122(3):1486–1501, 2007.
- [2] Michael J Buckingham. Wave speed and attenuation profiles in a stratified marine sediment: Geo-acoustic modeling of seabed layering using the viscous grain shearing theory. *The Journal of the Acoustical Society of America*, 148(2):962–974, 2020.
- [3] Michael J. Buckingham and Stephen A. S. Jones. A new shallow-ocean technique for determining the critical angle of the seabed from the vertical directionality of the ambient noise in the water column. *The Journal of the Acoustical Society of America*, 81(4):938–946, 1987.
- [4] George V. Frisk. *Chapter 5: The Method of Normal Modes*, page 110–163. P T R Prentice-Hall, 1994.
- [5] Charles W Holland, Jan Dettmer, and Stan E Dosso. Some reflections on buckingham’s viscous grain shearing model. *The Journal of the Acoustical Society of America*, 146(4.Supplement):2857–2857, 2019.
- [6] C. L. Pekeris. THEORY OF PROPAGATION OF EXPLOSIVE SOUND IN SHALLOW WATER. In *Geological Society of America Memoirs*, pages 1–116. Geological Society of America, 1948.
- [7] Jay Spendlove, Tracianne B Neilsen, and Mark K Transtrum. Information geometry analysis example for absolute and relative transmission loss in a shallow ocean. *Journal of the Acoustical Society of America, Express Letters*, 2024.

- [8] Evan K. Westwood and Robert A. Koch. Elimination of branch cuts from the normal-mode solution using gradient half spaces. *The Journal of the Acoustical Society of America*, 106(5):2513–2523, 1999.
- [9] Evan K. Westwood, C. T. Tindle, and N. R. Chapman. A normal mode model for acousto-elastic ocean environments. *The Journal of the Acoustical Society of America*, 100(6):3631–3645, 1996.